

Statistical State Dynamics based study of turbulence in Eady fronts. Part 1. Instability

Eojin Kim[†], Brian F. Farrell¹

¹Department of Earth and Planetary Sciences, Harvard University, Cambridge, MA 02138, USA

The streamwise roll and streak structure (RSS) is prominent in observations of the planetary boundary layer in the atmosphere and ocean and in unstratified wall-bounded shear flows. Although the RSS in these systems is structurally similar, the mechanism forming and maintaining the RSS in both remains controversial. This study demonstrates that the same turbulence-sustaining mechanism identified to underlie the RSS in the Statistical State Dynamics (SSD) formulation of unstratified wall-bounded shear flow dynamics (Farrell & Ioannou 2012; Farrell *et al.* 2016) also operates in the Eady front. We analyze the mechanism by which turbulence and symmetric instability interact to form the RSS in the baroclinic stratified Eady front model by adapting to the Eady front problem the stability analysis of the second order closure of the SSD used previously to study roll formation in unstratified wall-bounded shear flows. Our findings advance mechanistic understanding of RSS formation in the turbulent geostrophic front regime and establish foundational parallels between geophysical turbulent front dynamics and turbulence dynamics in engineering-scale shear flows.

Key words: statistical state dynamics, S3T, symmetric instability, front dynamics

1. Introduction

Fronts in geophysical flows (both ocean and atmosphere) are regions of enhanced horizontal density and velocity gradients that emerge ubiquitously in the planetary boundary layer (PBL) from the interplay among rotation, stratification, and shear flow dynamics which organizes the density and velocity fields into sharp interface zones in near geostrophic equilibrium. In the upper ocean, the PBL extends from the surface to depths of 10 to 100 meters and serves as the main interface for the exchange of heat, carbon and momentum between the atmosphere and the interior of the ocean, with the frontal areas acting as hotspots for these dynamical transport processes. These mixing processes are commonly associated with transport by roll-streak coherent and/or turbulent structures (RSS). The Eady problem (Eady 1949) provides a critical lens through which to examine the complex interplay between buoyancy and shear flow dynamics associated with the formation and equilibration of geostrophically balanced fronts and the interaction of these fronts with the RSS regime in the planetary boundary layer. The Eady model remains a cornerstone of geophysical fluid dynamics because it captures essential processes, while its formulation of the dynamics simplifies analysis of the mechanisms responsible. While simulating a vertically sheared zonal flow in thermal wind balance with a lateral temperature gradient, this model also captures the interaction between buoyancy and Reynolds stress forming the roll streak structure (RSS) that contributes prominently to mixing processes in frontal regions. This paper synthesizes the theoretical foundations of this turbulence regime in the Eady problem using statistical state dynamics (SSD) to

[†] Email address for correspondence: ekim@g.harvard.edu

identify the central role of the interplay between symmetric instability (SI) and turbulent Reynolds stresses in forming the RSS in a turbulent front.

Within the Eady model hydrodynamic instability manifests when the slope of potential temperature (θ) surfaces exceeds that of absolute momentum (M) surfaces, creating conditions for potential energy transfer to cross-frontal circulations. This specific instability mechanism, referred to as symmetric instability (SI), represents a fundamental mode of adjustment in baroclinic environments. The associated symmetric overturning circulations are responsible for a substantial component of the submesoscale structures observed in the PBL across diverse atmospheric and oceanic regimes. However, observational evidence indicates that baroclinic fronts in nature predominantly exhibit neutral or stable stratification with respect to symmetric instability. The degree of stability varies across different systems, ranging from marginally stable/neutral conditions (Emanuel 1988) to strongly stable (Mack & Schoeberlein 2003). Despite this variability in background stratification characteristics, coherent symmetric roll structures persist across a spectrum of stability conditions. Observations of the north wall of the gulf stream (Savelyev *et al.* 2018) suggest large symmetric circulations of order $0.7 - 1$ km exist from near the sea surface down to 5 km depth while SI theory would predict the appearance of symmetric circulations only down to 50 – 60 m depth (Thomas 2005). Moreover, while SI theory typically can only explain mixing down to 50 – 60m depth, observational data (Bosse *et al.* 2021) reveals subduction of phytoplankton and other tracers originating near the sea-surface down to 1km depth. The RSS structures responsible for these transport circulations manifest even under regimes strongly stable to symmetric instability, suggesting other dynamical roll-forming and maintaining mechanisms operate to form and maintain RSS in turbulent fronts.

Classical analyses of RSS turbulence formation and equilibration posit sequential evolution from laminar SI through Kelvin-Helmholtz secondary instabilities leading by potential vorticity (PV) adjustment to neutrality, often accompanied by inertial oscillations (Tandon & Garrett 1994; Stamper & Taylor 2016; Taylor & Ferrari 2009). This classical analysis has difficulty producing consistency with at least some observations. For example, sequential evolution is unable to predict equilibration at high Richardson number or to regimes strongly stable to laminar SI. Consistency with observations can be established by allowing for the role that emerging evidence suggests of a coupling between the Reynolds stress torque mechanism known to operate in unstratified shear flows (Farrell & Ioannou 2012) and the SI RSS growth mechanism. This study introduces a Statistical State Dynamics (SSD) framework to the Eady front problem which, through systematic separation of the SI modal growth mechanism from the Reynolds stress turbulence-mediated growth mechanism, reveals how symmetric roll structures can emerge from a synergy between SI and the Reynolds stress torque mechanism. The SSD we study has as control parameters Richardson number Ri , which controls the strength of the symmetric instability mechanism, and free stream turbulence ϵ , which controls the strength of the Reynolds stress torque mechanism. This separation of mechanism as a function of parameter choice allows us to advance understanding of frontal dynamics and equilibration in both ocean and atmospheric systems.

2. Eady model set up

The thermal and velocity structure of a geostrophically balanced front is described by the thermal wind relation linking the vertical shear of the geostrophic wind to the horizontal temperature gradient. Under the Boussinesq assumption density varies only

with temperature so buoyancy is a function of temperature. The thermal wind balance between zonal velocity and buoyancy is written as

$$\frac{dU_G(y)}{dy} = \frac{1}{f} \frac{db_G}{dz} \quad (2.1)$$

where f is the Coriolis parameter and we have used the convention that the x is the streamwise (zonal) direction, y is the wall normal (vertical) direction and z is the spanwise (meridional) direction with corresponding velocity u, v, w and unit vectors $\mathbf{i}, \mathbf{j}, \mathbf{k}$ respectively.

In the Eady model equilibrium state both the background vertical shear of the zonal velocity and the spanwise temperature gradient are constant throughout the domain. The total velocity and total buoyancy can be decomposed into the following form:

$$\underline{u}_T = U_G(y)\mathbf{i} + \underline{u}(x, y, z, t) \quad (2.2)$$

$$b_T = b_G(z) + b(x, y, z, t) \quad (2.3)$$

where $U_G(z)$ and $b_G(z)$ are the background velocity and buoyancy components consistent with thermal wind balance. In the Eady model equilibrium state these are written as follows:

$$b_G(z) = M^2 z \quad (2.4)$$

$$U_G(y) = \frac{M^2}{f} y \quad (2.5)$$

Corresponding equilibrium velocity \underline{u}_{Te} and buoyancy b_{Te} are:

$$b_{Te} = N^2 y + M^2 z \quad (2.6)$$

$$\underline{u}_{Te} = U_G(y)\mathbf{i} \quad (2.7)$$

where N^2 is the Brunt-Vaisala frequency.

Governing equations for \underline{u} and b are:

$$\frac{\partial \underline{u}}{\partial t} + (\underline{u}_T \cdot \nabla) \underline{u}_T = -\nabla \Pi - f \mathbf{j} \times \underline{u} + \nu \Delta \underline{u} + b \mathbf{j} \quad (2.8)$$

$$\frac{\partial b}{\partial t} + (\underline{u}_T \cdot \nabla) b + w M^2 = \kappa \Delta b \quad (2.9)$$

where $\Delta := (\partial_{xx} + \partial_{yy} + \partial_{zz})$ and w is the spanwise velocity component of \underline{u} . With the exception of taking x as the streamwise direction, y as the vertical (wall normal) direction, and z as the spanwise direction, this equation form is as in (Taylor & Ferrari 2010).

Velocity is non-dimensionalized by $M^2 H / f$; with the vertical length scale, H , taken to

be the height of the upper boundary this velocity scale corresponds to the shear across the domain in the vertical direction; consistently, time is nondimensionalized by f/M^2 . Nondimensional parameters are:

$$\Gamma = \frac{M^2}{f^2}, Re = \frac{H^2 M^2}{f\nu}, Ri = \frac{N^2 f^2}{M^4}, Pr = \frac{\nu}{\kappa} \quad (2.10)$$

corresponding to the Rossby, Reynolds, Richardson and Prandtl numbers respectively.

Nondimensionalized equations are

$$\frac{\partial \underline{u}}{\partial t} + (\underline{u}_T \cdot \nabla) \underline{u}_T = -\nabla \Pi - \frac{1}{\Gamma} \mathbf{j} \times \underline{u} + \frac{1}{Re} \Delta \underline{u} + Ri \cdot \mathbf{b} \mathbf{j} \quad (2.11)$$

$$\frac{\partial b}{\partial t} + (\underline{u}_T \cdot \nabla) b + w \frac{1}{Ri \cdot \Gamma} = \frac{1}{Re Pr} \Delta b \quad (2.12)$$

Our numerical simulation assumes periodic boundary conditions in both the streamwise direction x , and the spanwise direction z . Along the wall-normal direction, y , stress free and zero buoyancy flux conditions are applied at both the top and bottom. Other studies have used stress and buoyancy boundary fluxes to destabilize the symmetric instability by reducing the Richardson number (Taylor & Ferrari 2010; Haine & Marshall 1997). Our boundary conditions precluded this mechanism of driving the symmetric circulation.

Nondimensional equilibrium velocity and buoyancy are:

$$b_{Te} = y + \frac{1}{Ri \cdot \Gamma} z \quad (2.13)$$

$$\underline{u}_{Te} = y \mathbf{i} \quad (2.14)$$

3. SSD Formulation

Formulation of the SSD equations begins with decomposing variables into mean and fluctuation components. Velocity \underline{u} and buoyancy b decomposed into mean and fluctuations are:

$$\underline{u}(x, y, z, t) = \underline{U}(y, z, t) + \underline{u}'(x, y, z, t) \quad (3.1)$$

$$b(x, y, z, t) = B(y, z, t) + b'(x, y, z, t) \quad (3.2)$$

taking an overbar to denote a Reynolds average operator and capital letters to denote a Reynolds averaged variable, we indicate our choice of the streamwise average for our Reynolds average so that:

$$\bar{\underline{u}} = [\underline{u}]_x = U \quad (3.3)$$

$$\bar{b} = [b]_x = B \quad (3.4)$$

Our choice of the streamwise mean for our Reynolds average anticipates that the RSS instability will break the symmetry of our model in the spanwise direction and that this RSS can be conveniently isolated in the first cumulant by not including the spanwise

mean in the Reynolds average for our SSD. Equations for mean velocity \underline{U} and mean buoyancy B can be obtained by taking the streamwise mean of equation (2.11) and (2.12):

$$U_t = (U_y + 1)\Psi_z - U_z\Psi_y - \partial_y \overline{u'v'} - \partial_z \overline{u'w'} + \Delta_1 \frac{U}{Re} - \frac{\Psi_y}{\Gamma} \quad (3.5)$$

$$\Delta_1 \Psi_t = (\partial_{yy} - \partial_{zz})(\Psi_y \Psi_z - \overline{v'w'}) - \partial_{yz}(\Psi_y^2 - \Psi_z^2 + \overline{w'^2} - \overline{v'^2}) + \Delta_1 \Delta_1 \frac{\Psi}{Re} - Ri \cdot \frac{\partial B}{\partial z} + \frac{1}{\Gamma} \frac{\partial U}{\partial y} \quad (3.6)$$

$$B_t = -\left(\frac{1}{Ri \cdot \Gamma} + B_z\right)\Psi_y + B_y \Psi_z - \partial_y (\overline{b'v'}) - \partial_z (\overline{b'w'}) + \frac{1}{RePr} \Delta_1 B \quad (3.7)$$

in which $\Delta_1 := (\partial_{yy} + \partial_{zz})$ and where we have taken advantage of nondivergence in the spanwise/cross-stream plane to write the spanwise and cross-stream velocities in streamfunction form as $W = \frac{\partial \Psi}{\partial y}$ and $V = -\frac{\partial \Psi}{\partial z}$. Expressing our streamwise mean solution velocity component in terms of \underline{U} and Ψ isolates the RSS structures into the first cumulant.

Equations for the fluctuation components of velocity \underline{u}' and buoyancy b' are obtained by subtracting mean equation (3.5) – (3.7) from equations (2.11) and (2.12). The fluctuation velocity dynamics is expressed in the wall normal velocity and wall normal vorticity formulation in which nondivergence of velocity is intrinsically incorporated (Schmid & Henningson 2001).

Fluctuation velocity, vorticity and buoyancy are decomposed into streamwise wavenumber components as

$$v'(x, y, z, t) = \sum_k v'_k(y, z, t) e^{ikx} \quad (3.8)$$

$$\eta'(x, y, z, t) = \sum_k \eta'_k(y, z, t) e^{ikx} \quad (3.9)$$

$$b'(x, y, z, t) = \sum_k b'_k(y, z, t) e^{ikx} \quad (3.10)$$

We can now incorporate the fluctuation velocity equations in the wall normal velocity-vorticity formulation into our perturbation equations to obtain these equations in the compact form:

$$\frac{\partial \hat{\phi}_k}{\partial t} = A \hat{\phi}_k + \xi_k \quad (3.11)$$

in which the fluctuation state vector is:

$$\hat{\phi}_k = \begin{bmatrix} v'_k \\ \eta'_k \\ b'_k \end{bmatrix} \quad (3.12)$$

and we have parameterized the fluctuation-fluctuation nonlinear term by a stochastic noise process $\xi(t)$. We note that in applying this model to physical problems, this

stochastic noise process incorporates also any external sources of turbulent fluctuations.

The matrix of the dynamics is:

$$A = \begin{bmatrix} A_{11} & A_{12} & A_{13} \\ A_{21} & A_{22} & A_{23} \\ A_{31} & A_{32} & A_{33} \end{bmatrix} \quad (3.13)$$

$$A_{11} = L_{OS}(U + U_G) + \Delta^{-1}(LV_{11}(V) + LW_{11}(W)) \quad (3.14)$$

$$A_{12} = L_{C1}(U + U_G) + \Delta^{-1}(LV_{12}(V) + LW_{12}(W)) - \Delta^{-1}\left(\frac{1}{F}\partial_y\right) \quad (3.15)$$

$$A_{13} = Ri\Delta^{-1}\Delta_2 \quad (3.16)$$

$$A_{21} = L_{C2}(U + U_G) + LV_{21}(V) + LW_{21}(W) + \frac{1}{F}\partial_y \quad (3.17)$$

$$A_{22} = L_{SQ}(U + U_G) + Lv_{22}(V) + LW_{22}(W) \quad (3.18)$$

$$A_{23} = 0 \quad (3.19)$$

$$A_{31} = -\partial_y(B + b_G) + \partial_z(B + b_G)\Delta_2^{-1}\partial_{yz} \quad (3.20)$$

$$A_{32} = \partial_z(B + b_G)\Delta_2^{-1}(ik) \quad (3.21)$$

$$A_{33} = -(U + U_G)(ik) + \Psi_z\partial_y - \Psi_y\partial_z + \frac{1}{RePr}\Delta \quad (3.22)$$

where $\Delta_2 = (\partial_{xx} + \partial_{zz})$.

$L_{OS}(U + U_G)$ is the Orr Sommerfeld operator with $U + U_G$ the streamwise mean velocity. For details on the Orr-Sommerfeld-Squire form of the dynamics see (Farrell & Ioannou 2012). Details of component equations (3.14) – (3.18) are provided in the appendix.

Following the SSD formulation as outlined in (Farrell & Ioannou 2019), a deterministic Lyapunov equation can be obtained for the ensemble average fluctuation covariance, C , solely from knowledge of A and the noise process covariance $Q := \langle \xi\xi^\dagger \rangle$:

$$\frac{dC_k}{dt} = AC_k + C_kA^\dagger + \epsilon Q \quad (3.23)$$

$$C_k = \hat{\phi}_k\hat{\phi}_k^\dagger \quad (3.24)$$

where \dagger denotes Hermitian transpose. We note that it is the remarkable existence of this time-dependent Lyapunov equation that permits us to obtain a deterministic SSD.

Turning now to the equations for the mean, we note that the Reynolds stress terms appearing in the mean equations (3.5) – (3.7) can be obtained by a linear operator, L_{RS} , applied to the covariances C_k , of the fluctuations cf. (Farrell & Ioannou 2012). Taking account of this, the equations for the mean state can be expressed in compact notation as follows:

$$\Xi_t = G(\Xi) + \sum_k L_{RS} C_k \quad (3.25)$$

where $\Xi = [U, \Psi, B]^T$. In equation (3.25), G is:

$$G(\Xi) = \left[\begin{array}{c} (U_y + 1)\Psi_z - U_z\Psi_y + \Delta_1 \frac{U}{Re} - \frac{\Psi_y}{\Gamma} \\ \Delta_1^{-1}[(\partial_{yy} - \partial_{zz})(\Psi_y\Psi_z) - \partial_{yz}(\Psi_y^2 - \Psi_z^2) + \Delta_1 \Delta_1 \frac{\Psi}{Re} - Ri \cdot \frac{\partial B}{\partial z} + \frac{1}{\Gamma} \frac{\partial U}{\partial y}] \\ -(\frac{1}{Ri \cdot \Gamma} + B_z)\Psi_y + B_y\Psi_z + \frac{1}{RePr} \Delta_1 B \end{array} \right] \quad (3.26)$$

and the forcing by the fluctuation stresses at each k is:

$$L_{RS} C_k = \left[\begin{array}{c} -\partial_y \overline{u'v'}|_k - \partial_z \overline{u'w'}|_k \\ \Delta_1^{-1}[(\partial_{yy} - \partial_{zz})(-\overline{v'w'}|_k) - \partial_{yz}(\overline{w'^2}|_k - \overline{v'^2}|_k)] \\ -\partial_y(\overline{b'v'}|_k) - \partial_z(\overline{b'w'}|_k) \end{array} \right] \quad (3.27)$$

in which the fluctuation stress operator L_{RS} has been composed using these linear operators:

$$\begin{aligned} L_{u'}^k &= [-ik\Delta_2^{-1}\partial_y, \Delta_2^{-1}\partial_z, 0] \\ L_{v'}^k &= [I, 0, 0] \\ L_{w'}^k &= [-\Delta_2^{-1}\partial_{yz}, -ik\Delta_2^{-1}, 0] \\ L_{b'}^k &= [0, 0, I]. \end{aligned} \quad (3.28)$$

For instance, when a grid based method is used in both y and z :

$$\overline{u'v'}|_k = \text{diag}(L_{u'}^k C_k L_{v'}^{k\dagger}) \quad (3.29)$$

The other stress terms are written in a similar manner. Note that stress terms $\sum_k L_{RS} C_k$ are linear in C_k .

We use for our RSS stability analysis an SSD closed at second order the formulation of which is referred to as S3T. This SSD consists of the first and second cumulant together with a stochastic closure. The S3T equations can be written compactly as:

$$\Xi_t = G(\Xi) + \sum_k L_{RS} C_k \quad (3.30)$$

$$\frac{dC_k}{dt} = AC_k + C_k A^\dagger + \epsilon Q.$$

While many choices exist for Q , we choose white in kinetic energy i.e. to excite each degree of freedom equally in kinetic energy so that buoyancy fluctuations arise from velocity fluctuations but are not directly excited. This is accomplished by choosing Q as follows (Farrell & Ioannou 2012):

$$Q = M^{-1} \quad (3.31)$$

$$M = (L_{u'}^{k\dagger} L_{u'}^k + L_{v'}^{k\dagger} L_{v'}^k + L_{w'}^{k\dagger} L_{w'}^k) / (2 * Ny * Nz) \quad (3.32)$$

This completes the formulation of the SSD. We now turn our attention to analyzing the stability of this system.

4. S3T stability formulation

In order to study stability, we first need to establish equilibrium states for which the time derivative of equations (3.30) vanish:

$$\Xi_e = \begin{bmatrix} U_e \\ \Psi_e \\ B_e \end{bmatrix} \quad (4.1)$$

$$C_e = \sum_k C_{ke}$$

Stability properties of these SSD equilibria Ξ_e , $\sum_k C_{ke}$ can be found by linearizing equation (3.30) around these equilibria. Taking free stream turbulence parameter $\epsilon = 0$ recovers the laminar Eady model equilibrium in which $U_e = 0, \Psi_e = 0, B_e = y$ with $\sum_k C_{ke} = 0$ with $U_{Te}(y) = U_e + U_G = y$ and $\bar{b}_{Te}(y, z) = B_e + b_G = y + \frac{1}{Ri \cdot \Gamma} z$. When ϵ increases the equilibrium streamwise mean flow $U_e(y)$ and $U_{Te}(y)$ departs from the laminar Eady model equilibrium. The resulting SSD equilibrium state $(\Xi_e, \sum_k C_{ke})(Ri, \epsilon)$ is a function of both Ri and the background turbulence intensity controlled by the parameter ϵ . Linear perturbation equations linearized around the SSD equilibrium state $(\Xi_e, \sum_k C_{ke})$ are:

$$(\delta \Xi)_t = \sum_i \frac{\partial G}{\partial \Xi_i} \big|_{\Xi_e} \delta \Xi_i + \sum_k L_{RS} \delta C_k \quad (4.2)$$

$$(\delta C_k)_t = A_{keq} \delta C_k + \delta C_k A_{keq}^\dagger + \delta A_k C_{keq} + C_{keq} \delta A_k^\dagger \quad (4.3)$$

where

$$\delta A_k = A_k(\Xi_e + \delta \Xi) - A_k(\Xi_e) \quad (4.4)$$

equations (4.2) and (4.3) comprise the formulation of the linear perturbation S3T dynamics. Having chosen to characterize our front model by parameters $Re = 400$, $\Gamma = 1$, $Pr = 1$, the remaining adjustable parameters in these equations are Richardson number Ri and background turbulence excitation intensity ϵ . Q is scaled such that $\epsilon = 1$ results in volume averaged RMS perturbation velocity being 1% of the maximum velocity of Eady model

profile. Explicitly, Q is scaled so that $\sqrt{2 \langle E_k \rangle} = 0.01$ where $\langle E_k \rangle = \text{trace}(M_k C_k)$ represents ensemble average kinetic energy density of the perturbation field as shown in (Farrell & Ioannou 2012).

This formulation allows us to identify an instability process fundamentally distinct from traditional hydrodynamic instability. While the S3T framework incorporates laminar modal instabilities isolated in the first cumulant (the mean flow), its primary advance is including instabilities arising from interactions between the mean flow and the fluctuations, that is equations (4.2) and (4.3), which are the first and second cumulants of our S3T SSD. This destabilization of the RSS is due to the remarkable fact that, in the presence of a streamwise streak, the background turbulence field is systematically strained to produce Reynolds stresses with torque organized to drive a roll circulation that is collocated with the instigating streak (Farrell *et al.* 2022; Nikolaidis *et al.* 2024). The S3T SSD formulation of the Eady front problem incorporates both SI and this Reynolds stress (RS) torque feedback instability mechanism. Mean equation (3.36) decoupled from the covariance equation contains the familiar dynamics of pure SI in the Eady model. The RS torque instability has been previously shown using the S3T formulation to identify RSS instabilities arising solely from interactions between the mean flow and the fluctuations in unstratified wall bounded shear flow (Farrell & Ioannou 2012; Farrell *et al.* 2016). Comprehensive understanding of the dynamics of the RSS in the turbulent Eady model requires taking account of both the traditional SI mechanism contained in the mean flow equation and also the RS torque mechanism arising from coupling between the mean flow equation and the fluctuation covariance equation.

5. RSS instability in the S3T SSD

This section presents our findings on RSS instability in the Eady model from numerical implementation of the S3T perturbation equations. The section is organized in three parts. In the first part, we examine the RSS instability supported solely by the RS torque mechanism, which can be isolated from SI because it continues to operate at Richardson numbers greater than unity where the SI instability vanishes. The RS torque mechanism thus provides an explanation for the commonly observed occurrence of RSS and attendant vertical transport in frontal regions with subcritical Ri for SI. In the second part, analysis of the interaction between the SI and RS torque mechanisms is made through parametric control of the growth rate of each of these roll forming mechanisms. In the third part, we demonstrate that the turbulence-mediated RS torque feedback mechanism continues to operate at $Ri < 1$. In order to demonstrate this, traditional hydrodynamic instabilities of the Eady model (SI, baroclinic instability, and mixed instability) are suppressed.

Our Numerical implementation uses $Ny = 21$ and $Nz = 40$ collocation points at $Re = 400$, $\Gamma = 1$, $Pr = 1$. Convergence was verified by doubling resolution. The computational domain spanned $Ly = 1$ vertically and $Lx = 1.75\pi$ streamwise, while the spanwise length Lz was systematically doubled from $Lz = 1.2\pi$ until adequate spanwise extent was obtained to capture the essential physics at each Ri (Wienkers *et al.* 2022b). The Lz/Lx ratio was chosen to be multiples of $1.2/1.75$ which aligns with conditions for resolving RSS excited by the RS torque mechanism in prior studies (Farrell & Ioannou 2012).

5.1. RSS instability supported by RS torque mechanism for ($Ri \geq 1$)

Traditional modal instability theories require $Ri < 1$ for RSS formation as symmetric instability does not exist for $Ri > 1$ and baroclinic instabilities have non-zero streamwise wavenumbers ($k_x \neq 0$) which is incompatible with roll structures. However, our study of roll streak formation in turbulent flows using the S3T formulation reveals an alternative

pathway to roll formation that continues to operate with $Ri > 1$. An advantage of this composite S3T formulation is that both SI (operating at $Ri < 1$) and the RS torque instability (which exists independent of Ri) are included in the analysis. Shown in figure 1 is RSS structure and stability at $Ri = 1$ which demonstrates that the RS torque instability supports roll-streak structure formation even when all SI are stable. This finding challenges the assumption that $Ri \geq 1$ precludes symmetric circulation structure formation.

The RS torque mechanism destabilizes transient optimals, and consistently the structures destabilized by the RS torque mechanism at Richardson number greater than unity exhibit the structure of transient optimals as found in (Zemskova *et al.* 2019). Traditional analyses of the Eady problem associate baroclinic instability with maximum growth rates at Richardson numbers greater than unity (Stone 1966). However, recent studies have revealed that transient optimal perturbations demonstrate zonally symmetric circulation patterns across both $Ri < 1$ and $Ri > 1$ regimes, challenging conventional stability paradigms (Zemskova *et al.* 2019). Baroclinic instability exhibits strong growth rates in $Ri > 1$ conditions through convective instability mechanisms characterized by finite group velocities when the streamwise mean flow velocity is zero, whereas roll circulations are absolutely unstable under these conditions. We note that all physical fronts have finite length so that the only instability that physical fronts support is that with zero group velocity. Moreover, baroclinic growth is dominated on frontal formation time scales by the growth of optimal perturbations not by the asymptotic growth rate of the exponential mode and in many cases optimals may not be present during the frontal formation time interval, a classical example of a nearly optimal perturbation for baroclinic wave excitation that is sometimes observed being short-wave phasing between the front and an upper level vorticity maximum of small scale, which only occurs occasionally. These considerations imply that in many cases baroclinic instability does not fundamentally influence roll formation in the $Ri < 1$ regime. Previous studies have focused on regions with Richardson number less than unity or with negative potential vorticity (necessary and sufficient conditions for SI in traditional formulations, respectively) when studying RSS formation. However, our results show that the RSS can arise in a broader class of flows and through a novel mechanism, suggesting a new approach to understanding roll circulations and transport in frontal regions. Moreover, while previous studies generally assume quasi-geostrophy when $Ri > 1$ (Pateras & Bakas 2017), this assumption needs careful reconsideration, as it precludes the class of RSS forced by RS. While other studies (Taylor & Ferrari 2010; Thomas *et al.* 2013; Haine & Marshall 1997) have used stress and buoyancy boundary flux to drive forced symmetric instability (FSI) by reducing the Richardson number, our results, which preclude this mechanism, show this mechanism is not necessary to drive the symmetric circulation.

In this subsection, we showed that the RS torque instability can give rise to RSS at $Ri \geq 1$ where the SI is not supported. The following subsection investigates the case when both the RS torque and the SI instabilities exist which occurs for $Ri < 1$.

5.2. Interaction between SI and RS torque instability

The S3T system of equations can be modified by including Rayleigh damping r_s in the mean equation allowing us to vary the growth rate of SI, which is contained in the mean equation. The resulting mean perturbation equation is:

$$(\delta\Xi)_t = \sum_i \left[\left[\frac{\partial G}{\partial \Xi_i} \right]_{\Xi_e} - r_s \right] \delta\Xi_i + \sum_k L_{RS} \delta C_k \quad (5.1)$$

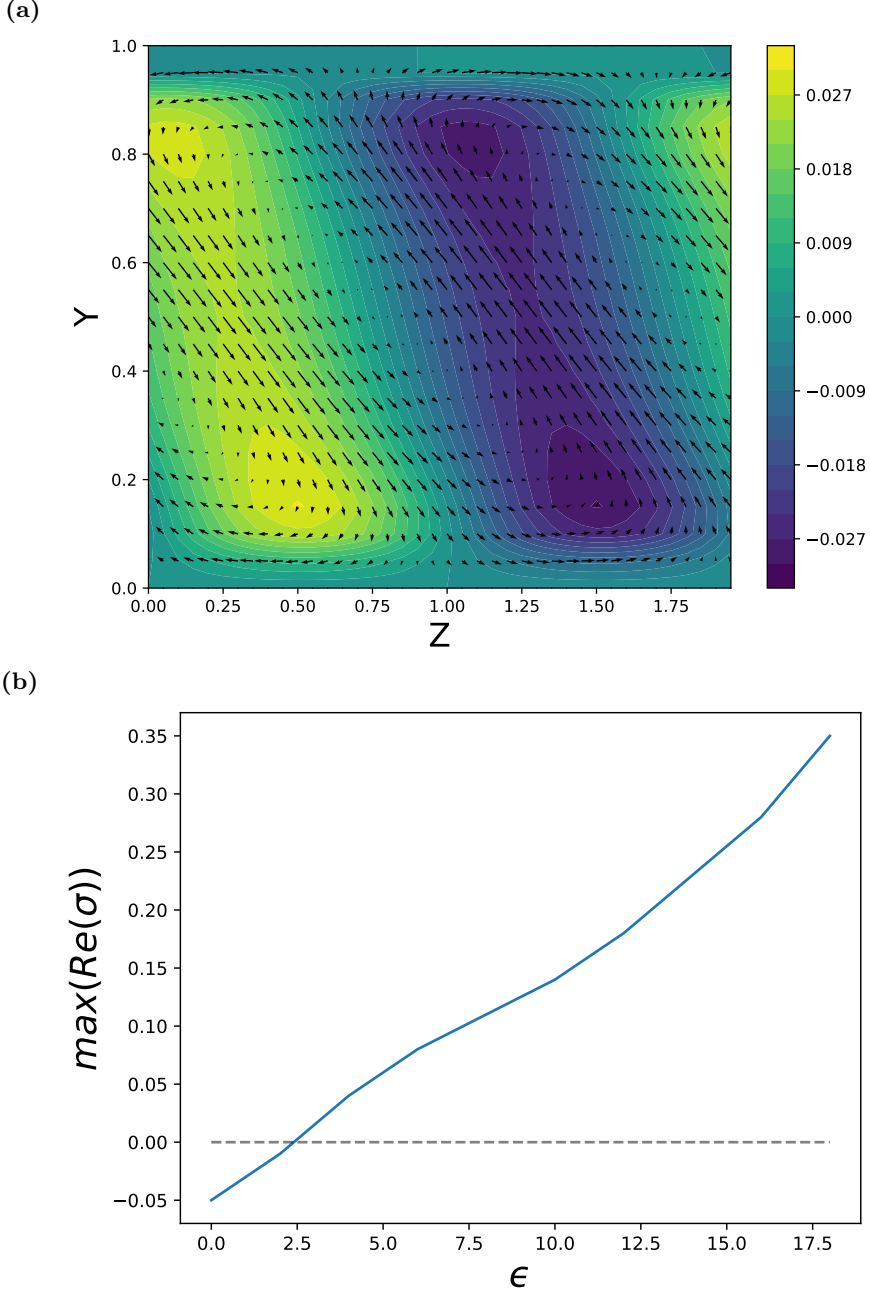


Figure 1: S3T analysis of RS torque-mediated RSS instability at $Ri = 1$. (a) RSS of the S3T eigenmode with maximum growth rate $Re(\sigma)$. Color contours show streak velocity δU while vectors show roll velocities $(\delta V, \delta W)$ (b) Stability diagram showing S3T RSS eigenmode growth rate $\max(Re(\sigma))$ as function of turbulence excitation parameter ϵ .

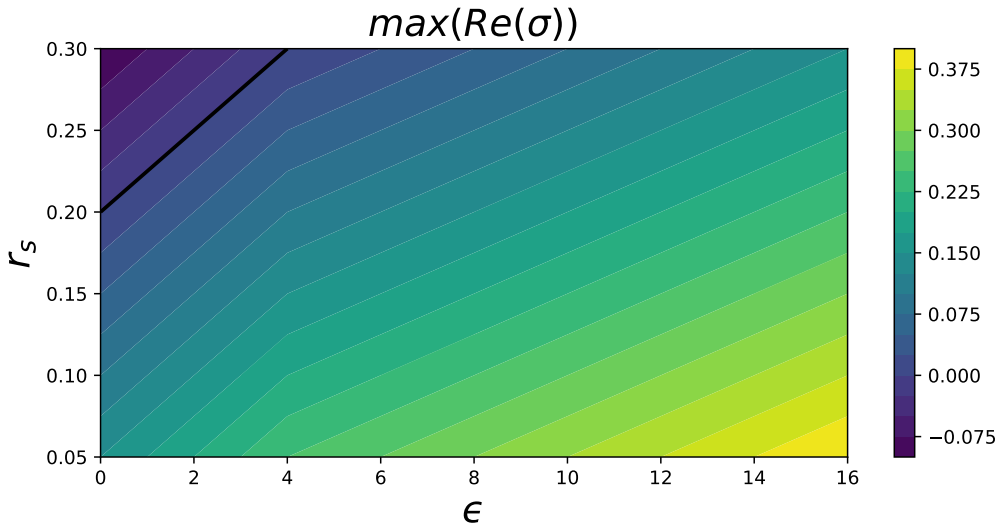


Figure 2: Stability diagram showing interaction between the SI and RS torque RSS destabilization mechanisms. The RS mechanism is controlled by ϵ while the SI mechanism is controlled by r_s . Contours show growth rate $max(Re(\sigma))$. The black line indicates neutral stability

As mentioned above, growth rate of the RS torque mechanism can be controlled by varying the background turbulence excitation parameter ϵ in the perturbation covariance equation. Together these parameters allow us to adjust the strength of the SI and RS torque instability independently. For simplicity we take the unperturbed Eady profile as the basic state for our stability analysis. Considering that smaller r_s implies greater support for SI while larger ϵ implies greater support for the RS torque instability mechanism we can interpret figure 2 to show the synergy between these instabilities.

The Richardson number Ri also affects the SI. A stability diagram in $1 - Ri$ and ϵ parameter space is shown in figure 3. Greater values of $1 - Ri$ imply greater support for the SI mode while greater values of ϵ imply greater support for the RS torque mode.

When $\epsilon = 0$ the RS torque mechanism is not supported and SI crosses the stability boundary for $(1 - Ri)$ marginally exceeding zero, corresponding to Richardson numbers slightly below unity. This is consistent since there is some viscous dissipation present in the problem; for instance, Stone found SI becomes stable when $Ri > 0.95$ in his study (Stone 1966).

It can be seen in figure 3 that Ri and ϵ synergistically interact to give rise to roll circulation with the overall shape of the stability diagram being qualitatively similar to figure 2. This is expected, as both r and Ri determine the strength of SI support.

5.3. Isolation of the Reynolds stress mediated RS instability by suppression of symmetric, baroclinic, and mixed instabilities

SI has been widely accepted as the primary mechanism responsible for generating RSS in frontal regions. In this section, we isolate the RS torque feedback mechanism in the Eady model by suppressing the other hydrodynamic instabilities supported by the Eady model including symmetric, baroclinic, and mixed modes. The S3T dynamics with

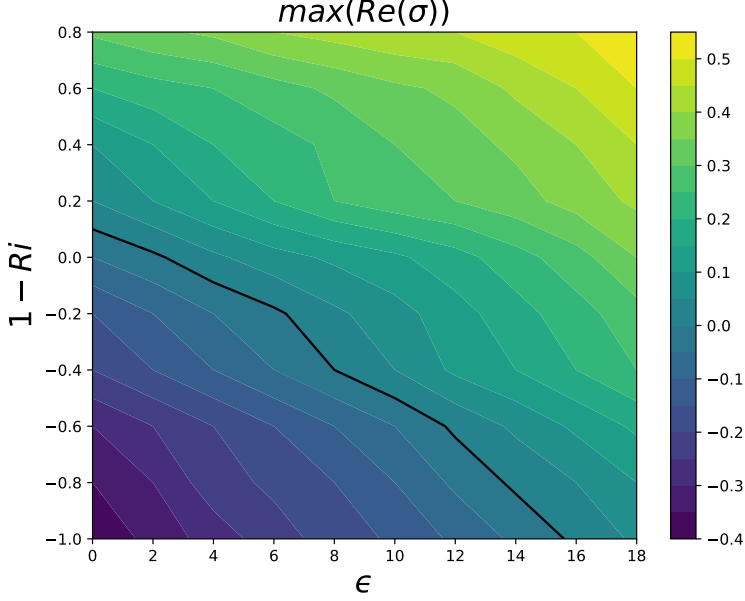


Figure 3: Stability diagram showing dependence of SI and RS torque instability on Ri and ϵ . Contours show growth rate $\max(\text{Re}(\sigma))$. The black line indicates neutral stability

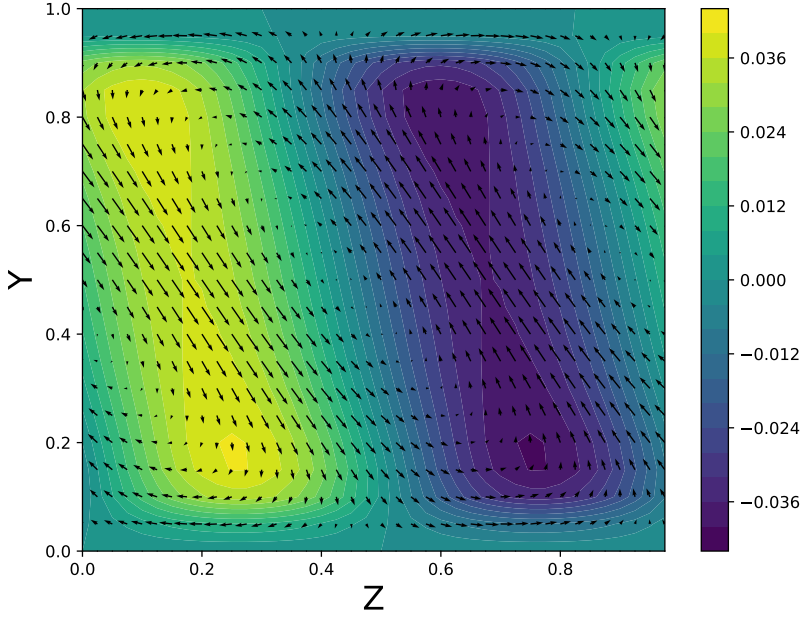
suppression of laminar hydrodynamic instabilities is indicated by noting by $\lambda < 0$ where modal instabilities have been capped:

$$(\delta \Xi)_t = \sum_i \left[\frac{\partial G}{\partial \Xi_i} (\lambda < 0) \right]_{\Xi_e} \delta \Xi_i + \sum_k L_{RS} \delta C_k \quad (5.2)$$

$$(\delta C_k)_t = A_{ke} (\lambda < 0) \delta C_k + \delta C_k A_{ke} (\lambda < 0)^\dagger + \delta A_k C_{ke} + C_{ke} \delta A_k^\dagger \quad (5.3)$$

in which suppression of SI is indicated by $\sum_i \left[\frac{\partial G}{\partial \Xi_i} (\lambda < 0) \right]_{\Xi_{eq}}$ while suppression of baroclinic and mixed instabilities is indicated by $A_{ke} (\lambda < 0)$ and $A_{ke} (\lambda < 0)^\dagger$. These instabilities were suppressed by capping the real part of all eigenvalues at -0.1 i. e. eigenvalues exceeding this threshold were adjusted to -0.1 to eliminate linear growth modes. This approach aligns with several previous studies of turbulent roll-streak dynamics, where analogous stabilization techniques were employed (Lozano-Duran *et al.* 2016, 2020). Shown in Figure 4 is roll circulation structure supported solely by the RS torque mechanism along with the stability diagram obtained at Richardson number $Ri = 0.25$. Despite suppressing all other modal instabilities supported by the Eady model, our analysis reveals roll formation persists driven purely by Reynolds stress torque. While suppressing all other modal instabilities (including symmetric instability) ensures roll formation arises purely from the Reynolds Stress (RS) torque mechanism, the resulting roll circulations exhibit structural similarities to those produced by SI. In both cases, rolls follow isopycnal surfaces in the interior before completing their circulation near the boundary. However, the mechanisms driving these similar structures are fundamentally different. From parcel exchange theory, SI relies on buoyancy energetics in which a dynamically allowed parcel exchange results in decrease in the mean flow

(a)



(b)

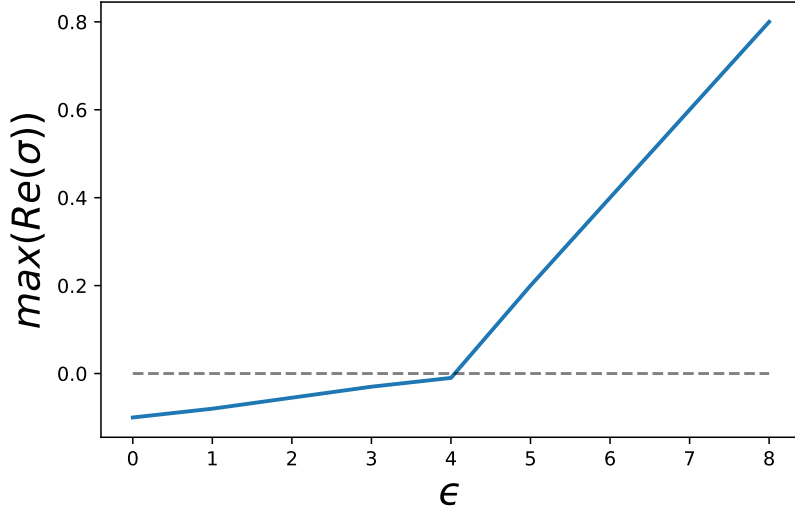


Figure 4: S3T RS torque mode stability analysis at $Ri = 0.25$ with suppression of all other instabilities. (a) Structure of the dominant S3T RSS eigenmode with maximum growth rate $Re(\sigma)$. Contours indicate streak velocity δU , while vectors indicate roll velocities $(\delta V, \delta W)$ (b) S3T RS torque mode stability diagram showing growth rate $\max(Re(\sigma))$ as a function of background turbulence intensity parameter ϵ . Dashed line represents the stability boundary.

gravitational potential energy with that energy accruing to the parcel, consistently, SI can be supported only when $Ri < 1$. Unlike SI, the RS torque mechanism relies on energy extracted by transient growth of perturbations contained in the background turbulence. This mechanism extracts kinetic energy from the energy of the mean flow and does not require buoyancy energetics nor the requirement for buoyancy energetics, $Ri < 1$. Our result aligns with the finding of (Zemskova *et al.* 2019), in which non-normal transient optimals manifest as symmetric circulations along buoyancy surfaces at all Richardson numbers. We can regard the RS torque as supplying the feedback required to destabilize these transient optimals. Our result showing support for roll forming instability by the RS torque mechanism without support for SI confirms that the dynamics behind these two roll forming mechanisms is fundamentally different. Even when initial $Ri < 1$, observed isopycnal-aligned rolls should not be automatically attributed to symmetric instability. Parameter regimes (such as background turbulence intensity and Richardson number) determine whether the RS torque destabilization dominates the initial formation of the rolls. Depending on the parameter regime, RSS may arise predominantly due to the RS torque mechanism.

In the appendix, we present a simple analytical dynamics illustrating the mechanism by which RS torque feedback destabilizes roll circulations using a modification of the lift-up matrix model for roll formation in unstratified boundary layers.

6. Conclusion

This study extended SI theory to incorporate the RS torque instability as a mechanism for roll circulation formation in frontal regions. By applying the S3T SSD to the Eady front model we reformulated that model into a SSD framework which allowed us to analytically unify the SI and RS torque mechanism to elucidate their roles in the Eady front problem. Our results demonstrate that roll circulations in frontal zones can arise independently by the RS torque mechanism, even in the absence of symmetric instability. Numerical implementations of the S3T formulation confirmed that the RS torque mechanism forms roll structures without reliance on modal hydrodynamic instabilities (SI, baroclinic instability, and mixed mode instability). Some of our key findings include that the SI and RS torque mechanisms cooperate to amplify roll formation. Importantly, the RS torque mechanism supports roll circulation at $Ri > 1$ in contrast to SI, which is suppressed under such conditions. Moreover, we have shown that background turbulence can support RSS for $Ri > 1$, this finding has implications for vertical transport and mixing in oceanographic frontal regions, where $Ri > 1$ is typical. Recent observational evidence (Ostrovksy *et al.* 2024) demonstrates that a large level of background turbulence persists even at Ri values approaching 10, suggesting that the Reynolds stress torque feedback mechanism could be active as a critical RSS formation mechanism under these high stratification conditions. This conclusion gains further support from multi-basin observational evidence. Southern Ocean hydrographic data (Forryan *et al.* 2013) confirm the ubiquity of $Ri > 1$ conditions alongside persistent meridional circulations – features irreconcilable with SI dynamics. The collective evidence implicates the RS torque mechanism for roll generation in strongly stratified frontal zones. Observations from the Sargasso Sea thermocline (Mack & Schoeberlein 2003) reveal inverse Richardson numbers approaching zero across much of the domain – a direct indicator of $Ri \gg 1$ stratification. Moreover, observations reveal roll structures near fronts exhibit lateral scales an order of magnitude larger than SI predictions (Perez *et al.* 2010), with cell widths consistently exceeding those compatible

with subcritical Richardson numbers. These observations could be explained by the RS torque RSS formation mechanism which has no scale except that imposed by the boundaries. Our findings from the S3T formulation applied to the Eady problem provide critical insights into the dynamics of roll circulation formation in atmospheric and oceanic frontal systems. The primary focus of this study was on characterizing S3T instabilities within turbulent Eady fronts under the SSD framework, but these results also provide a foundational framework for probing broader aspects of RSS dynamics in turbulent flows; among these are the equilibration of fronts and the maintenance of turbulent RSS states, both of which will be explored in the second part of this paper.

7. Appendix

7.1. Details of equation (3.14) – (3.18)

Here are the details of the operators presented in equation (3.14) – (3.18)

$$\begin{aligned}
LV_{11}(V) &= (k^2 V_y - V_{yzz} + k^2 V \partial_y - V_{zz} \partial_y - 2V_{yz} \partial_z - V_y \partial_{zz} - 2V_z \partial_{yz} - V \partial_{yzz}) \\
&\quad + [(ik)(V_y \partial_y + V \partial_{yy})](-ik \Delta_2^{-1} \partial_y) \\
&\quad + (k^2 V_z - V_{zzz} + V_{yz} \partial_y + V_z \partial_{yy} + V_y \partial_{yz} + V \partial_{yyz} - 2V_{zz} \partial_z - V_z \partial_{zz})(-\Delta_2^{-1} \partial_{yz}) \\
LW_{11}(W) &= (k^2 W \partial_z + W_{yy} \partial_z + W_y \partial_{yz} + W_{yyz} + W_{yz} \partial_y - W_{zz} \partial_z - 2W_z \partial_{zz} - W \partial_{zzz}) \\
&\quad + (ikW_y \partial_z + ikW \partial_{yz})(-ik \Delta_2^{-1} \partial_y) \\
&\quad + (2W_{yz} \partial_z + 2W_z \partial_{yz} + W_{zzy} + W_{zz} \partial_y + W_y \partial_{zz} + W \partial_{zzy})(-\Delta_2^{-1} \partial_{yz}) \\
LV_{12}(V) &= [(ik)(V_y \partial_y + V \partial_{yy})](\Delta_2^{-1} \partial_z) \\
&\quad + (k^2 V_z - V_{zzz} + V_{yz} \partial_y + V_z \partial_{yy} + V_y \partial_{yz} + V \partial_{yyz} - 2V_{zz} \partial_z - V_z \partial_{zz})(-ik \Delta_2^{-1} \partial_z) \\
LW_{12}(W) &= (ikW_y \partial_z + ikW \partial_{yz})(\Delta_2^{-1} \partial_z) \\
&\quad + (2W_{yz} \partial_z + 2W_z \partial_{yz} + W_{zzy} + W_{zz} \partial_y + W_y \partial_{zz} + W \partial_{zzy})(-ik \Delta_2^{-1} \partial_z) \\
LV_{21}(V) &= -(V_z \partial_y + V \partial_{yz})(-ik \Delta_2^{-1} \partial_y) + (ikV \partial_y)(-\Delta_2^{-1} \partial_{yz}) \\
LW_{21}(W) &= (ikW_y) - (W_z \partial_z + W \partial_{zz})(-ik \Delta_2^{-1} \partial_y) + (ik)(W_z + W \partial_z)(-\Delta_2^{-1} \partial_{yz}) \\
LV_{22}(V) &= -(V_z \partial_y + V \partial_{yz})(\Delta_2^{-1} \partial_z) + (ikV \partial_y)(-ik \Delta_2^{-1} \partial_z) \\
LW_{22}(W) &= -(W_z \partial_z + W \partial_{zz})(\Delta_2^{-1} \partial_z) + (ik)(W_z + W \partial_z)(-ik \Delta_2^{-1} \partial_z)
\end{aligned} \tag{7.1}$$

7.2. Simple modified lift-up matrix model for RSS formation

In this section, a simple modification of the matrix model of the lift-up process responsible for roll formation in wall-bounded shear flows is extended to illustrate the coupling between the SI and the RS torque mechanism for roll formation in frontal regions. Due to buoyancy coupling, roll formation in an Eady front cannot be represented by the familiar 2 by 2 lift-up matrix dynamics framework using only velocity components u and v as in the case of unstratified shear flow. Instead, the system requires a three-variable formulation involving u , ψ (the streamfunction characterizing roll structures), and b . Under the assumption of an unbounded domain in the wall-normal direction y , mean equation (3.36) decoupled from the covariance equation can be written as:

$$\partial_t \begin{bmatrix} u \\ \psi \\ b \end{bmatrix} = \begin{bmatrix} -\nu k^2 & S(ik_z) - \Omega(ik_y) & 0 \\ -\Omega(\frac{ik_y}{k^2}) & -k^2\nu & 1 \\ 0 & N^2(ik_z) - S * \Omega(ik_y) & -\kappa k^2 \end{bmatrix} \begin{bmatrix} u \\ \psi \\ b \end{bmatrix} \quad (7.2)$$

where $k^2 = k_z^2 + k_y^2$. Given the unbounded domain in the y-direction, we can assume solutions of the form $[u, \psi, b]^T e^{ik_z z} e^{ik_y y}$. The vertical shear of the background streamwise velocity is characterized by a constant shear rate, $\frac{dU}{dy} = S$. With these model choices, the nondimensionalized modified lift-up matrix model for the dynamics (7.2) can be written as:

$$\partial_t \begin{bmatrix} u \\ \psi \\ b \end{bmatrix} = \begin{bmatrix} -\frac{1}{Re} k^2 & (ik_z) - \frac{1}{\Gamma}(ik_y) & 0 \\ -\frac{1}{\Gamma}(\frac{ik_y}{k^2}) & -k^2 \frac{1}{Re} & 1 \\ 0 & Ri(ik_z) - \frac{1}{\Gamma}(ik_y) & -\frac{1}{RePr} k^2 \end{bmatrix} \begin{bmatrix} u \\ \psi \\ b \end{bmatrix} \quad (7.3)$$

The RS torque instability mechanism can be incorporated into this dynamics by introducing a feedback parameter, ζ , that couples the streamwise streak with the roll velocity components:

$$v_t \sim -\zeta u, w_t \sim \zeta u \quad (7.4)$$

This coupling induces a rotational torque that drives the roll circulation streamfunction, ψ , modeling the RS torque from the second cumulant of the S3T SSD. The resulting modified lift-up matrix incorporating ζ modeling the RS torque is:

$$\partial_t \begin{bmatrix} u \\ \psi \\ b \end{bmatrix} = \begin{bmatrix} -\frac{1}{Re} k^2 & (ik_z) - \frac{1}{\Gamma}(ik_y) & 0 \\ -\frac{1}{\Gamma}(\frac{ik_y}{k^2}) - \zeta \frac{(ik_y + ik_z)}{k^2} & -k^2 \frac{1}{Re} & 1 \\ 0 & Ri(ik_z) - \frac{1}{\Gamma}(ik_y) & -\frac{1}{RePr} k^2 \end{bmatrix} \begin{bmatrix} u \\ \psi \\ b \end{bmatrix} \quad (7.5)$$

dimensionless parameters Γ and Pr will be set to unity, ($\Gamma = 1, Pr = 1$), for this analysis.

Eigenanalysis of the modified lift-up matrix equation (7.5) reveals a most unstable mode with eigenvalue:

$$\lambda = -\frac{(k_y^2 + k_z^2)}{Re} + \frac{[(k_y^2 + k_z^2)[\zeta(k_y^2)[\frac{k_z^2}{k_y^2} - 1] + k_y^2(\frac{k_z}{k_y} - 1) + ((Rik_z - k_y)(k_z^2 + k_y^2)) * i]^{1/2}}{k_y^2 + k_z^2} \quad (7.6)$$

These equations can be further simplified under the condition of isopycnal motion, in which fluid parcels adhere to surfaces of constant density. This requires parcel trajectory satisfy the relationship:

$$\frac{\partial b}{\partial z} dz + \frac{\partial b}{\partial y} dy = 0 \quad (7.7)$$

$$\frac{dy}{dz}|_b = -\frac{\frac{\partial b}{\partial z}}{\frac{\partial b}{\partial y}} = -\frac{1}{\Gamma \cdot Ri} = -\frac{1}{Ri} \quad (7.8)$$

Adopting solution form $be^{ik_z}e^{ik_y}$ isopycnal trajectories require wavenumbers satisfy:

$$\frac{\frac{\partial b}{\partial z}}{\frac{\partial b}{\partial y}} = \frac{k_z}{k_y} = \frac{1}{Ri} \quad (7.9)$$

With adoption of the isopycnal trajectory constraint, the expression for the most unstable eigenvalue, λ , becomes:

$$\lambda = -\frac{(k_y^2 + k_z^2)}{Re} + \frac{[(k_y^2 + k_z^2)[(\zeta(\frac{1}{Ri} + 1) + 1)k_y^2(\frac{1}{Ri} - 1)]]^{1/2}}{k_y^2 + k_z^2} \quad (7.10)$$

The dynamics of roll structures in stratified turbulent flows exhibit notable behavior when cells are constrained to move along isopycnals. Under this constraint, the imaginary component within the square root term of the eigenvalue equation vanishes, resulting in a purely real eigenvalue. This implies the absence of phase speed in roll-streak structures, consistent with stationary patterns observed in direct numerical simulations and field observations of frontal regions. Moreover, disappearance of the imaginary part of the eigenvalue aligns with the zero phase speed of lift-up transient optimal perturbations in flows with zero background spanwise velocity ($W = 0$) (Butler & Farrell 1992). While the RS torque feedback mechanism preferentially destabilizes roll circulations with zero spanwise phase speed, the vanishing imaginary component of the most unstable eigenvalue also emerges as a direct consequence of the isopycnal-motion constraint. For a given Ri and roll wavelength, the critical feedback, ζ , required for destabilization can be quantitatively determined. If dissipation is ignored, destabilization requires:

$$(\zeta(\frac{1}{Ri} + 1) + 1)k_y^2(\frac{1}{Ri} - 1) > 0 \quad (7.11)$$

The above expression can be decomposed into two components corresponding to the RS torque mechanism.

$$(\zeta(\frac{1}{Ri} + 1))k_y^2(\frac{1}{Ri} - 1) \quad (7.12)$$

and the SI mechanism:

$$k_y^2(\frac{1}{Ri} - 1) \quad (7.13)$$

Parameterization of the RS torque by ζ in the modified lift-up equation enables

explicit separation of the contributions to destabilization of RSS by SI and the RS torque mechanisms.

REFERENCES

- BACHMAN S.D., KEMPER B. F., TAYLOR J.R. & THOMAS L.N. 2017 Parameterization of Frontal Symmetric Instabilities. I: Theory for Resolved Fronts. *Ocean Modeling* **109** 72-95
- BOSSE A., TESTOR P., DAMIEN P., ESTOURNEL C., MARSALEIX P., MORTIER L., PRIEUR L. & TAILLANDIER V. 2022 Wind-Forced Submesoscale Symmetric Instability around Deep Convection in the Northwestern Mediterranean Sea. *Fluids* **6** 123
- BUTLER, K. M. & FARRELL, B. F. 1992 Three-dimensional optimal perturbations in viscous shear flows. *Phys. Fluids* **4**, 1637–1650.
- CONSTANTINO, N. C., LOZANO-DURÁN, A., NIKOLAIDIS, M.-A., FARRELL, B. F., IOANNOU, P. J. & JIMÉNEZ, J. 2014*b* Turbulence in the highly restricted dynamics of a closure at second order: comparison with DNS. *J. Phys. Conf. Ser.* **506**, 012004.
- LOZANO-DURAN A., NIKOLAIDIS M. A., CONSTANTINO N. C. & KARP M. 2019 Wall turbulence without modal instability of the streaks. *arXiv:1909.05490*
- LOZANO-DURAN A., CONSTANTINO N. C., NIKOLAIDIS M. A. & KARP M. 2020 Cause-and-effect of linear mechanisms sustaining wall turbulence. *J. Fluid Mechanics* **914** A8 1-A8 58
- EADY E.T. 1949 Long Waves and Cyclone Waves. *Tellus* 33-52
- EMANUEL, K. 1988 Observational Evidence of Slantwise Convective Adjustment. *Amer. Meteo. Soci* **116** 1805-1816
- FARRELL, B. F. & IOANNOU, P. J. 2012 Dynamics of streamwise rolls and streaks in turbulent wall-bounded shear flow. *J. Fluid Mech.* **708**, 149–196.
- FARRELL, B. F. & IOANNOU, P. J. 2016 Structure and mechanism in a second-order statistical state dynamics model of self-sustaining turbulence in plane Couette flow. *Phys. Rev. Fluids* (submitted, arXiv:[1607.05020](#)).
- FARRELL, B. F., IOANNOU, P. J. & M.-A., NIKOLAIDIS 2016 Instability of the roll/streak structure induced by free-stream turbulence in pre-transitional Couette flow. *Phys. Rev. Fluids* (submitted, arXiv:[1607.05018](#)).
- FARRELL B. F., IOANNOU P. J. & NIKOLAIDIS M. A. 2018 Parametric mechanism maintaining Couette flow turbulence is verified in DNS. *Center for Turbulence Research Proceedings of the Summer Program 2018*
- FARRELL, B. IOANNOU, P 2019 Statistical State Dynamics: A New Perspective on Turbulence in Shear Flow. *Zonal Jets Phenomenology, Genesis, and Physics. Ed. Boris Galperin and Peter L. Read. Cambridge University Press 2019.* 380-400.
- FARRELL B. F., IOANNOU P. J. & NIKOLAIDIS M. A. 2022 Mechanism of Roll-Streak Structure Formation and Maintenance in Turbulent Shear Flow. *arXiv:2205.07469*.
- FORRYAN A., MARTIN A. P., SROKOSZ M. A., POPOVA E. E., PAINTER S. C. & RENNER A. H. H. 2013 A new observationally motivated Richardson number based mixing parametrization for oceanic mesoscale flow. *J. Geophysical Research: Oceans* **118** 1405-1419
- HAINE, T. W. N. & MARSHALL J. 1997 Gravitational, Symmetric, and Baroclinic Instability of the Ocean Mixed Layer. *J. Physical Oceanography* **28** 634-658
- MACK, S.A. & SCHOEERLEIN H.C. 2003 Richardson Number and Ocean Mixing: Towed Chain Observations. *J. Physical Oceanography* **34** 736-754
- NIKOLAIDIS M. A., IOANNOU P. J. & FARRELL B. F. 2024 Fluctuation covariance-based study of roll-streak dynamics in Poiseuille flow turbulence. *J. Fluid Mechanics* **988** A14.
- OSTROVSKY L., SOUSTOVA I., TROITSKAYA Y. & GLADSKIKH D. 2024 Evolution of small-scale turbulence at large Richardson numbers. *Nonlin. Processes Geophys.* **31** 219-227
- PATERAS S.C. & BAKAS N.A. 2017 Transient Growth of Ageostrophic Perturbations in a Baroclinic Shear Flow. *Perspectives on Atmospheric Sciences* 377-384
- PEREZ R.C., CRONIN M.F. & KESSLER W.S. 2010 Tropical Cells and a Secondary Circulation near the Northern Front of the Equatorial Pacific Cold Tongue*. *J. Physical Oceanography* **40** 2091-2106
- SAVELYEV, I., THOMAS, L, SMITH, G.B., WANG Q., SHEARMAN, R. K., HAACK, T., CHRISTMAN

- A. J., BLUMQUIST B., SLETTEN M., MILLER, W.D. & FERNANDO H.J.S. 2018 Aerial Observations of Symmetric Instability at the North Wall of the Gulf Stream *Geophysical Research Letters* **45**, 236-244
- SCHMID, P. J. & HENNINGSON, D. S. 2001 *Stability and Transition in Shear Flows*. Springer, New York.
- STAMPER M & TAYLOR J 2016 The transition from symmetric to baroclinic instability in the Eady model. *Ocean Dynamics* **67**, 65-80.
- STONE, P 1966 On non-geostrophic baroclinic stability. *J. Atmospheric. Sciences*. **23**.
- STONE, P 1970 On non-geostrophic baroclinic stability: Part ii. *J. Atmospheric. Sciences*. **27**.
- STONE, P 1971 Baroclinic stability under non-hydrostatic conditions. *J. Fluid. Mech.* **45**.
- TANDON, A & GARRETT, C 1994 Mixed layer restratification due to a horizontal density gradient. *J. Phys. Oceanogr.* **24**, 1419-1424.
- TAYLOR, J & FERRARI, R 2009 On the equilibration of a symmetrically unstable front via a secondary shear instability. *J. Fluid Mech* **622**, 103-113.
- TAYLOR, J & FERRARI, R 2009 Buoyancy and Wind-Driven Convection at Mixed Layer Density Fronts. *J. Phys. Oceanogr.* **40**, 1222-1242.
- THOMAS, L. N. 2005 Destruction of Potential Vorticity by Winds. *J. Physical. Oceanography* **35** (5), 2457-2466.
- THOMAS, L. N., TAYLOR J. R., FERRARI R. & JOYCE T. M. 2013 Symmetric instability in the Gulf Stream. *Deep Sea Research Part II Topical Studies in Oceanography* **91**, 96-110.
- THOMAS, L. N., TAYLOR J. R., D'ASARO, E. A., KLYMAK, J. M. & SHCHERBINA, A. 2016 Symmetric Instability, Inertial Oscillations, and Turbulence at the Gulf Stream Front. *J. Physical Oceanography* **46**, 197-217.
- TREFETHEN, L. N. & EMBREE M. 2005 Spectra and Pseudospectra: The Behavior of Nonnormal Matrices and Operators. *Princeton University Press, Princeton*
- WIENKERS, A., THOMAS, L. & TAYLOR J. 2022a The influence of front strength on the development and equilibration of symmetric instability. Part 1. Growth and saturation. *J. Fluid Mech.* **926**.
- WIENKERS, A., THOMAS, L. & TAYLOR J. 2022b The influence of front strength on the development and equilibration of symmetric instability. Part 2. Nonlinear evolution. *J. Fluid Mech.* **926**.
- ZEMSKOVA, V , PASSAGGIA, P ,& WHITE B 2019 Transient energy growth in the ageostrophic Eady model. *J. Fluid. Mech.* **885**, 1419-1424.
- ZHOU H., DEWAR W., YANG W., LIU H., CHEN X., LI R., LIU C. & GOPALAKRISHNAN G. 2022 Observations and modeling of symmetric instability in the ocean interior in the Northwestern Equatorial Pacific. *Commun Earth Environ* **3** 28